AIAA JOURNAL
Vol. 36, No. 10, October 1998

Modeling Ascent Configurations of Strained High-Altitude Balloons

Frank Baginski*
George Washington University, Washington, D.C. 20052
and
Kenneth A. Brakke†
Susquehanna University, Selinsgrove, Pennsylvania 17870

We consider the problem of estimating stresses in the ascent shape of an elastic high-altitude scientific balloon. The balloon envelope consists of a number of long, flat, tapered sheets of polyethylene called gores that are sealed edge-to-edge to form a complete shape. Because the film is so thin, it has zero bending stiffness and cannot support compressions. In particular, the balloon film forms internal folds of excess material when the volume is not sufficiently large. Because of these factors, a standard finite element approach will have difficulty computing partially inflated balloon shapes. In our approach, we develop a variational principle for computing strained balloon shapes that incorporates regions of folded material as a part of the geometric model. We can apply our model to fully inflated or partially inflated configurations. The equilibrium shape is the solution of minimum energy satisfying a given volume constraint. We apply our model to a design shape representative of those used in scientific ballooning and compute a family of ascent configurations with regions of external contact for a volume as low as 22% of its float value.

Nomenclature

$\mathcal{C}_k$	= class of piecewise differentiable surfaces with symmetry of the dihedral group D_k
D_k	= dihedral group; the group of motions of the plane generated by rotations about the origin through an angle of $2\pi/k$ and reflections about some fixed axis
E	= Young's modulus of balloon film
e	= balloon film thickness
K_{tape}	= stiffness constant for load tape (units of force)
$N_{\mathcal{T}}$	= number of facets in a triangulation of $\mathcal{S}_f$
n_c	= number of circumferential fibers
n_g	= number of gores in a complete balloon
$(R_d(s), 0, Z_d(s))$	= generating curve for design shape, where s is arc length, $0 \le s \le \ell_d$
$r_{1,\max}$	= $\max_i x_{i,1}$
$r_{2,\max}$	= $\max_i (x_{i,2}^2 + y_{i,2}^2)^{1/2}$
$\mathcal{S}_f$	= reference configuration corresponding to $\mathcal{S}_f$
$\mathcal{S}$	= complete balloon surface
$\mathcal{S}_f$	= fundamental section of a balloon shape
$\mathcal{S}_f'$	= reflection of $\mathcal{S}_f$ in the xz plane
$\mathcal{S}_f(v_{i,j})$	= fundamental section of a balloon shape defined by the set of vertices $\{v_{i,j}\}$
T_l	= facet in S_f
$\mathcal{T}_l$	= facet in $\mathcal{S}_f$
$\lvert u \rvert$	= $\sqrt{(u_1^2 + u_2^2 + u_3^2)}$, where u is (u_1, u_2, u_3)
$\mathcal{V}$	= gas volume enclosed by $\mathcal{S}$
$\mathcal{W}^k$	= $\{(x, y, z) \in R^3 \mid 0 \le y \le \tan(\pi/k)x\}$
w_{film}	= weight density of balloon film
w_{tape}	= weight density of load tape
ν	= Poisson's ratio of balloon film

I. Introduction

THE design shape of a large scientific balloon is typically based on an axisymmetric model that was developed by researchers at the University of Minnesota in the 1950s (Ref. 1). A solution of this model is referred to as a Σ shape. If one assumes that all of the tension is carried in the meridional direction and that the circumferential stresses are zero, one obtains the so-called natural-shape design.[2] We will consider a balloon design based on a variation of the natural-shape design, where the weight of the caps and load tapes is included in the axisymmetric balloon envelope model. We will assume that the weight due to all other structures (such as venting ducts, fins, inflation tubes, backup tapes, etc.) is included in the payload that is located at the base of the balloon.

Although the utility of the natural shape has been established by numerous successful missions using balloons based on the Σ-shape design, the model has a number of limitations. In particular, the length of the generating curve is assumed to be inextensible, and the shape is assumed to be in static equilibrium. In a real balloon at float, the film is strained, and the hoop stresses are not necessarily zero. Near the top of the balloon, the film is under biaxial tension and behaves like a standard membrane. Below this region, the tension is predominantly in the meridional direction and the circumferential tension is negligible. As the gas bubble decreases, the balloon envelope collapses, and the portion of the balloon that behaves like a standard membrane becomes smaller. The balloon film cannot support a compressive load, and so the film will wrinkle and form internal folds of excess material.

At float, an elastic balloon will stretch and take on a shape that is slightly taller and smaller in diameter than its design configuration. In the lower portion of the balloon, where the tension is predominantly in the meridional direction, the film will undergo contraction in the circumferential direction due to Poisson's effect. Strained float shapes and a family of ascent shapes were considered in Ref. 3, using a variation of the model presented here. For float conditions, a standard finite element method applied to a shell model (see, e.g., Ref. 4) would predict small compressive stresses in the bottom portion of the membrane. If the negative circumferential stresses are negligible, one could obtain a reasonable first approximation to the stresses in the film for the special case at float. However, for shapes even slightly below float, this method would lead to poor results because the higher compressive stresses would suggest a stiffness in the film that is unfounded. In our approach, internally folded material, regions of small or zero circumferential tensions, and the contraction due to Poisson's effect are handled by our geometric model, and we are able to consider shapes well below the float altitude. Ascent shapes are characterized by large

Received Nov. 3, 1997; revision received June 23, 1998; accepted for publication July 3, 1998.

*Associate Professor, Department of Mathematics. Member AIAA.
†Professor, Department of Mathematics.

deformations but relatively small strains. We consider ascent shapes in the range $0.22 \le \mathcal{V}/\mathcal{V}_d \le 1.00$, where $\mathcal{V}$ is the volume of the shape and $\mathcal{V}_d$ is the volume of the design shape. Even though the range of volumes considered here is large, the corresponding altitude variation is comparatively small. Suppose a balloon enclosing a volume of $\mathcal{V}_d = 29.5 \times 10^6$ ft^3 with a specific buoyancy ($b_d = 2.2539$e-04 lbf/ft^3) is at a float altitude of 129,362 ft. By Archimedes' principle, the total lift of the balloon is $b_d \mathcal{V}_d = 6649$ lbf, where subscript d indicates a parameter related to the design shape. A decrease in volume to $\mathcal{V} = 0.22\mathcal{V}_d$ with buoyancy $b = b_d \mathcal{V}_d/\mathcal{V} = 1.0782$e-03 lbf/ft^3 (preserving $b\mathcal{V} = b_d \mathcal{V}_d$) corresponds to a lower altitude of 99,101 ft. (The relation between altitude and buoyancy is tabulated in Ref. 5.) This comparatively small altitude variation is due to the low density of air at these altitudes.

Wrinkling in the balloon film is negligible in comparison to the magnitudes of typical folds that are observed. In this paper, we will include a model for folds and ignore wrinkling in the balloon fabric. Although large deformations of membrane-like structures have been studied theoretically and experimentally (see, e.g., Fig. 18.20, Ref. 6), the loading conditions and size of a typical large scientific balloon are nonstandard, especially the partially inflated configurations. In particular, because the actual balloon film is so thin (0.8-mil polyethylene is a typical balloon film material), any reasonably sized model would require an extremely thin material.[7] For example, in a model with a gore length of 6 ft, the material would be 8.0e-06 in. thick. These are reasons to develop an accurate mathematical model that is representative of how a real balloon behaves.

Any finite element method applied to large scientific balloons will need to address the presence of negative compressive stresses. For example, Schur[8] computed strained balloon shapes at the float altitude using ABAQUS, removing compressions through the use of a tension field. Note that our approach in this paper is fundamentally different from that of a tension field. Tension field theory normally deals with finely wrinkled membranes (see, e.g., Ref. 9). However, for problems that we are interested in, the folds of excess material are of significantly higher magnitude. In the special case of float conditions, we find that the tension field approach[8] and our own approach lead to the same solution for the strained float shape.[7] The advantage of our approach is that we can apply our strain energy methods to ascent shape geometries with large regions of folded material that cannot be handled by standard finite element methods. In this paper, ascent shapes are quasisteady-state equilibria, in the sense that they are computed for a fixed altitude. We do not consider the dynamics of the balloon flight. Although actual ascent geometries include a variety of other large-scale structures (cyclic lobe patterns, flat wing-like sections of collapsed balloon film hanging beneath the gas bubble), we will focus on cyclic shapes without regions of internal contact that can be determined by studying a single half-gore. We include new results on strained partially inflated balloon shapes in the range $0.22 \le \mathcal{V}/\mathcal{V}_d \le 1.00$. Our goals are to estimate the shape of the balloon (including folds where they are present) and to determine estimates of the stress distribution for a variety of ascent shapes. For the range of shapes here, the stresses in the exterior film surrounding the gas bubble and load tapes are most important inasmuch as these structures carry the bulk of the balloon system weight.

Balloon shapes with large-scale features including a spherical top, internally folded balloon fabric, a periodic lobe pattern surrounding the gas bubble, and flat wing-like structures below the gas bubble were considered in Refs. 10 and 11. Variational principles were developed to model the geometries of fully inflated and partially inflated configurations. The total energy of the balloon system was modeled as the sum of the hydrostatic pressure potential due to the lifting gas and the weight of the balloon film. By minimizing this energy subject to a volume constraint and certain material constraints, the authors were able to compute solutions, called energy minimizing shapes (EM shapes), that possessed many features observed in real balloons. The results in Refs. 10 and 11 demonstrated the feasibility of utilizing a variational approach for computing balloon shapes. However, these models were concerned primarily with the geometry of balloon shapes and distribution of folded material. The straining in the balloon film and load tapes was ignored. In Ref. 7, the authors considered strained balloon shapes but only for float conditions and with a model that restricted degrees of freedom for vertices along the center of the deformed gore. In the present work, a geometric model is used that utilizes more degrees of freedom along the center of the gore.

In reality, the balloon film is a nonlinear viscoelastic material, but we will model it as a linearly elastic material with a constant strain model, using material properties typical of what would be expected for the float conditions. We ignore the stress response history of the balloon's ascent to float altitude. In our model, the balloon surface is triangulated, using the gore structure as a fundamental element. A flat reference configuration is associated with each gore in the balloon shape, and so it is possible to associate a triangle in the balloon surface with a unique triangle in the flat reference configuration. A constant strain model is used to compute the strain energy for the faceted balloon surface. An isotropic plane–stress constitutive model is used to estimate the stress distribution. The load tapes that run along the edges of the gores are modeled as linearly elastic strings. The contributions to the gravitational potential energy that are due to the weight of the load tapes and two external caps are also included in the variational principle. The external caps are modeled as an added thickness. One could incorporate finite elements more sophisticated than the linear elements used here. However, in the case of the float conditions where we can directly compare our results with those computed by other methods, we find that we obtained good results using linear elements and a constant strain model.[7] For this reason, we retain linear elements.

To compute a family of strained balloon shapes, we begin with the initial design shape and evolve a strained float shape. We then solve a series of constrained minimization problems, decrementing the volume at each step, obtaining a family of ascent shapes. At each stage, the EM shape from the previous step is used as the initial guess for the new volume. Because the balloon will deform from its design shape, a small internal fold of excess material will form along the center of each gore at float. As the volume decreases, the length and depth of the fold increase. It is difficult to determine the precise length and depth of the actual fold, and this makes the problem of estimating the stresses in the fold region even more difficult. For example, the wrinkling in certain regions of the fold could be of a higher amplitude than the wrinkling in the neighboring regions consisting of exterior facets. However, our model does provide an estimate of the location and size of the fold in the reference configuration. The specifics of our model are discussed in Sec. II. The volumes considered here are sufficiently large to avoid internal contact, and so we need not consider shapes with wing sections. We find that internal contact occurs near $\mathcal{V} = 0.22\mathcal{V}_d$.

The validity of our approach was established for the fully deployed configuration in Ref. 7, and in this paper, we focus on ascent configurations that can be modeled by a half-gore. The design criteria are based primarily on conditions the balloon will encounter at float. Among the strained shapes, at or near float (for example, $0.85 \le \mathcal{V}/\mathcal{V}_d \le 1.00$), the maximum film stresses occur at $\mathcal{V} = \mathcal{V}_d$. Beginning with the float altitude, we find that the maximum principal stresses decrease initially with decreasing volume. However, once the gas bubble gets sufficiently small (for example, $\mathcal{V} < 0.58\mathcal{V}_d$), the maximum stresses increase with decreasing volume. In particular, we find that the maximum principal stresses for the shape $\mathcal{V} = 0.22\mathcal{V}_d$ are larger than the maximum principal stresses for the float shape $\mathcal{V} = \mathcal{V}_d$.

In Sec. III, we formulate a variational principle that includes gravitational potential energy and strain energy. In Sec. IV, we compute a numerical EM shape for float and a number of ascent shapes. In Sec. V, we present some concluding remarks.

II. Geometric Model

Before attempting to model the strain in a partially inflated balloon shape, a model for the geometry of the balloon envelope that is representative of how a real balloon behaves is necessary. The model should incorporate features used in the construction of real balloons, such as the gore, external caps, and load tapes. A gore is a long, flat, tapered thin sheet of polyethylene. (For the design shape in Sec. IV, it is nearly 600 ft long, over 8 ft wide at the widest point, and 0.8 mil thick.) To make a complete shape, the gores are sealed edge to edge. Load tapes run along the gore seams from the top to the bottom of

the balloon. Normally, one, two, or three external caps cover the top 25–30% of the balloon. The gore structure is important in modeling partially inflated balloon shapes because internal folds form along the centers of these structures. The present model differs from that of Ref. 10 by including the strain energy of the film and load tapes. Although Ref. 3 considers strain energy, the model presented here allows for extra degrees of freedom for vertices that lie along the center of the deformed gore. These differences are outlined in the following subsections. For the convenience of the reader, we first review our geometric model of balloon shapes.

Real balloon shapes near float are not axisymmetric but exhibit a dihedral symmetry. In the following, let D_k be the dihedral group. D_k is the group of motions of the plane generated by rotations about the origin through an angle of $2\pi/k$ and reflections about some fixed axis. Looking down onto the top of a balloon with D_k symmetry and lining up the central axis of the balloon with the z axis, one could recognize a shape having the same symmetries as that of a regular polygon with k sides. In this work, k is equal to the the number of gores n_g. In Fig. 1, we present a balloon shape with eight gores and D_8 symmetry. In Refs. 10 and 11, the basic building block was the fundamental section $\mathcal{S}_f$, and in this paper, $\mathcal{S}_f$ refers to a deformed half-gore that is contained in the wedge-shaped region

$$\mathcal{W}^k = \{(x, y, z) \in R^3 \mid 0 \le y \le \tan(\pi/k)x\}$$

$\mathcal{S}_f$ will be approximated by a faceted surface and, with no loss of generality, will denote the faceted surface itself. $\mathcal{S}'_f$ is the mirror image of $\mathcal{S}_f$ and is obtained by reflecting $\mathcal{S}_f$ in the xz plane, i.e., if (x, y, z) is a vertex in $\mathcal{S}_f$, then $(x, -y, z)$ is a vertex in $\mathcal{S}'_f$. The complete shape $\mathcal{S}$ is assembled from k copies of $\mathcal{S}_f$ and k copies of $\mathcal{S}'_f$ using the symmetries of D_k. $\mathcal{C}_k$ will denote the class of balloon shapes with dihedral symmetry D_k, and $\mathcal{S}$ will denote a complete shape in $\mathcal{C}_k$. Because we are considering a single half-gore in this work, we will choose the convention that the deformed right gore edge will lie in the plane $y = \tan(\pi/k)x$. Any excess material will be treated as if it is contained within a fold lying in the xz plane. This is a rough approximation but consistent with what is observed in real balloons.

We first describe the geometry of a typical shape in $\mathcal{C}_k$. We do so by focusing on the geometry of a half-gore. In Fig. 1a, we present the right half of a flattened gore S_f with its tail located at the origin $(0, 0)$. In Fig. 1b, we present a curved but unstrained surface that is formed by bending S_f to conform to the design profile. The right edge of the gore lies in the plane $y = \tan(\pi/k)x$. No folds are present in Fig. 1.

To facilitate modeling the straining in a deformed gore, we will consider three configurations, S_f (Fig. 2), $\mathcal{S}_f$ (Fig. 3), and $\tilde{\mathcal{S}}_f$ (Fig. 4). The size of the fold is exaggerated for illustration purposes. S_f is the flat reference configuration, and $\mathcal{S}_f$ is the deformed gore with excess material folded into the xz plane. $\tilde{\mathcal{S}}_f$ is an auxiliary configuration that will be used to estimate the straining in the fold. The excess material in $\tilde{\mathcal{S}}_f$ is extended into the $y < 0$ region. In Fig. 4a, the excess material in $\tilde{\mathcal{S}}_f$ lies in the $y < 0$ region. The portion of Fig. 4a outlined in dots lies behind the xz plane and is identical with the exterior facets in Fig. 3a, forming the boundary of the gas bubble. If the faceted configuration S_f is deformed into $\mathcal{S}_f$ (or $\mathcal{S}_f$), the distortion will involve rigid-body displacements and in-plane straining of the facets that make up S_f. In Fig. 4, vertices labeled $v_{i,0}$, $v_{i,1}$, and $v_{i,2}$ are collinear, whereas in Fig. 3, the corresponding vertices $u_{i,0}$, $v_{i,1}$, and $v_{i,2}$ are not. The fold consisting of excess material in Fig. 3a is based on observations and is representative of how excess material is stored. However, when folding the material into the xz plane using $\mathcal{S}_f$, we find higher than expected stresses in folded facets. This was not as critical for the strained float shape because the folded region is very small (see Ref. 7, where straining of excess material was calculated after folding into the xz plane). We cannot ignore the straining in the fold. However, based on observations, it should be less than the straining in the exterior facets. If we estimate the straining of excess material using the representation in Fig. 4, we find that the circumferential and meridional stresses for facets of excess material in $\tilde{\mathcal{S}}_f$ are comparable to the magnitudes of immediately adjacent exterior facets (see Sec. IV). Because the distribution of folded material cannot be known exactly,

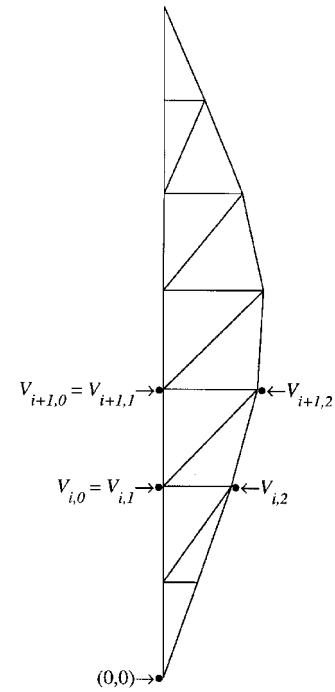

Fig. 1a S_f half-gore in the flat reference configuration.

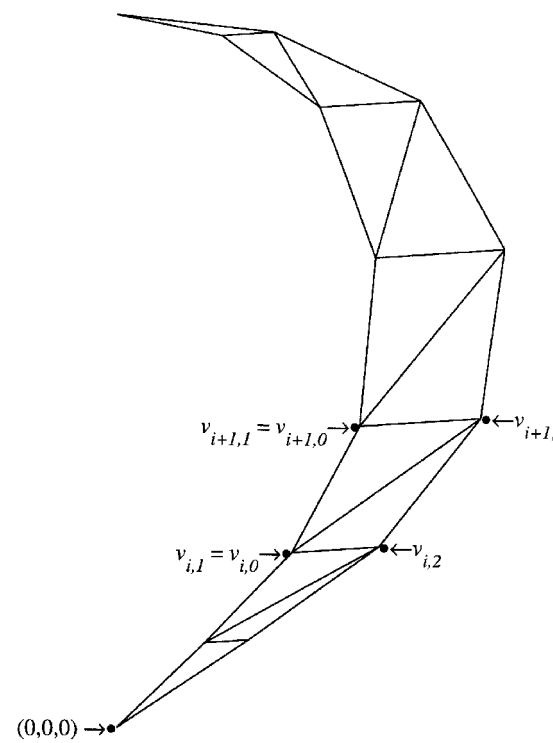

Fig. 1b S_f^0 unstrained initial configuration (no folds).

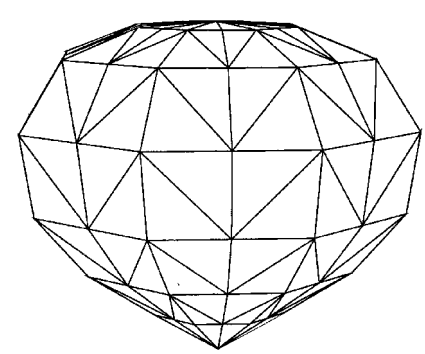

Fig. 1c Design shape.

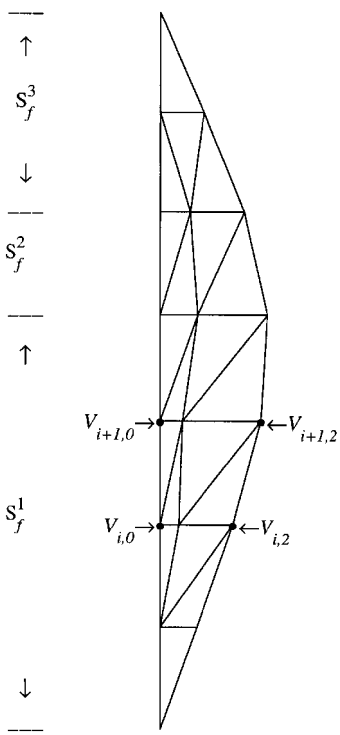

a) S_f half-gore in the flat reference configuration

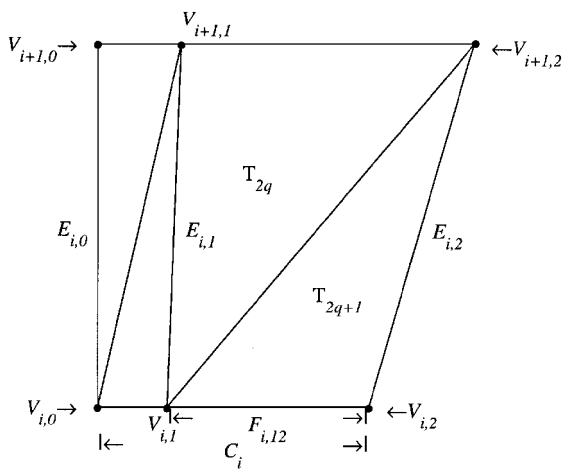

b) Quadrilateral between meridional station i and $i+1$

Fig. 2 S_f configuration.

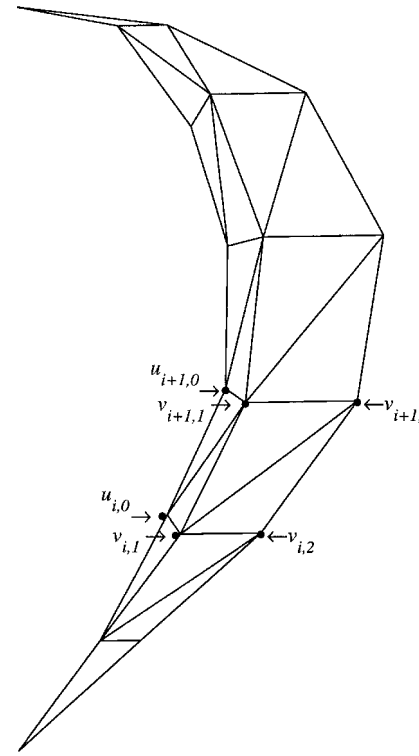

a) S_f deformed half-gore with excess material folded into xz plane

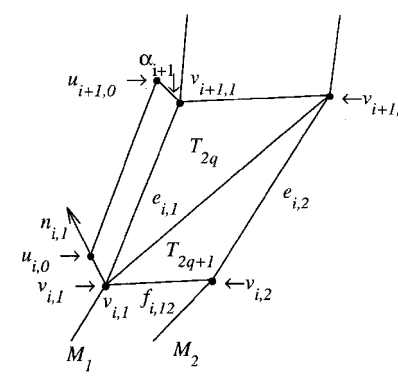

b) Deformed quadrilateral between meridional station i and $i+1$

Fig. 3 S_f configuration.

the strain energy in the folded material is better represented by $\tilde{\mathcal{S}}_f$ than by $\mathcal{S}_f$. The straining in the fold of the true balloon is most likely less than the estimate based on $\tilde{\mathcal{S}}_f$ (or $\mathcal{S}_f$). For these reasons, our strain energy computations for excess material will be based on $\tilde{\mathcal{S}}_f$. We will discuss this aspect of the model in Sec. V. In Figs. 2b, 3b, and 4b, we have selected typical sections of S_f, $\mathcal{S}_f$, and $\tilde{\mathcal{S}}_f$, respectively, and labeled important quantities that will be needed to describe the geometries of these configurations.

In all figures, we follow the convention that a vertex in the reference configuration is denoted by an uppercase V and a vertex in the deformed configuration will be denoted by a lowercase v. A vertex $V_{i,j}$ in $S_f \cup S_f'$ is identified with a vertex $v_{i,j}$ in $\mathcal{S}_f \cup \mathcal{S}_f'$ (or $\tilde{\mathcal{S}}_f \cup \tilde{\mathcal{S}}_f'$), where $j = 0, \pm 1, \pm 2$ and $i = 1, \ldots, n_c + 2$. Perpendicular to the center axis of a flat gore are the directed edges

$$C_i = V_{i,2} - V_{i,0}, \qquad i = 1, \ldots, n_c + 2$$

The subscript i is the station number along a meridian. Note that $C_1 = C_{n_c+2} = (0, 0)$. Along the right boundary of a gore are the directed edges,

$$E_{i,2} = V_{i+1,2} - V_{i,2} \tag{1}$$

Vertices $v_{i,2} = (x_{i,2}, y_{i,2}, z_{i,2})$ lie in the plane $y = \tan(\pi/k)x$, and

$$e_{i,2} = v_{i+1,2} - v_{i,2} \tag{2}$$

Because $y_{i,2} = \tan(\pi/k)x_{i,2}$, we say that $v_{i,2}$ has two degrees of freedom (corresponding to the free parameters $x_{i,2}$ and $z_{i,2}$). In previous models, e.g., Ref. 3, vertex $v_{i,1}$ had zero degrees of freedom because its position was determined by projecting $v_{i,2}$ onto the xz plane. In our treatment, we allow vertices $v_{i,0}$ to have three degrees of freedom, i.e.,

$$v_{i,0} = (x_{i,0}, y_{i,0}, z_{i,0}) \tag{3}$$

where $x_{i,0}$, $y_{i,0}$, and $z_{i,0}$ are free but $y_{i,0} \le 0$ (see Fig. 4). Vertex $v_{i,1}$ is the point located at the intersection of the xz plane and the line connecting $v_{i,0}$ and $v_{i,2}$.

The vertex at the top of the balloon has one degree of freedom because only its z component can vary. The vertex at the tail of the balloon is assumed to be fixed. By construction, the depth of the fold α_i at each circumferential station is given by $\alpha_i = |v_{i,0} - v_{i,1}|$. The curve that marks the center of the deformed gore is $\mathcal{M}_1$ and is defined by $\{v_{i,1}, i = 1, \ldots, n_c + 2\}$. The edge joining $v_{i+1,1}$ to $v_{i,1}$ is $e_{i,1} = v_{i+1,1} - v_{i,1}$. The load tape is located along the curve $\mathcal{M}_2$ that is defined by $\{v_{i,2}, i = 1, \ldots, n_c + 2\}$. The edge joining $v_{i,1}$ and $v_{i,2}$ is $f_{i,12} = v_{i,1} - v_{i,2}$.

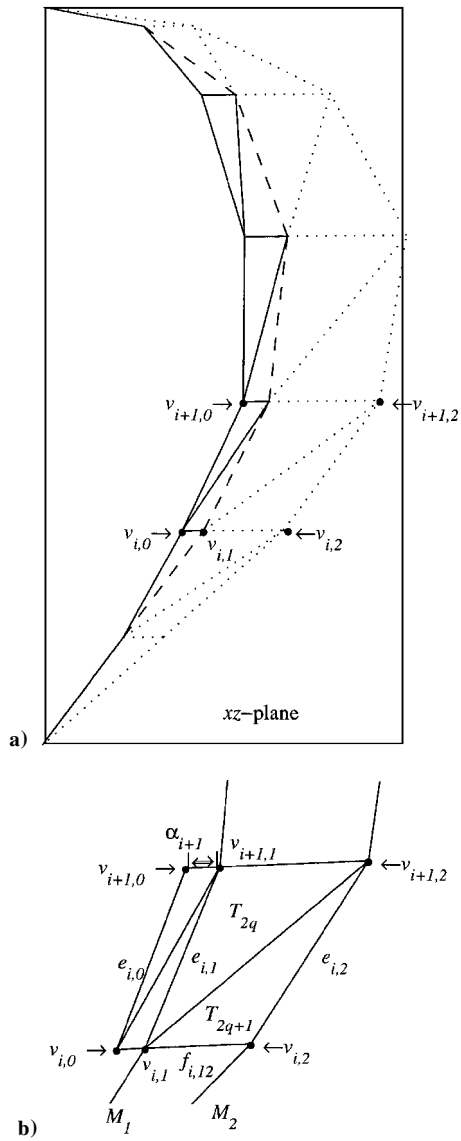

Fig. 4 $\tilde{S}_f$ configuration: a) $\tilde{S}_f$ deformed half-gore with excess material (outlined in solid and dashed edges) penetrating xz plane, triangles outlined in dotted lines lie in the region $y > 0$; and b) deformed quadrilateral between meridional station i and $i + 1$.

Vertices $v_{-2,i}$ and $V_{-2,i}$ are determined by symmetry, i.e., if $v_{i,2} = (x_{i,2}, y_{i,2}, z_{i,2})$ is a vertex in $\mathcal{S}_f$ (or $\tilde{\mathcal{S}}_f$), then $v_{i,-2} = (x_{i,2}, -y_{i,2}, z_{i,2})$ is a vertex in $\mathcal{S}'_f$ (or $\tilde{\mathcal{S}}'_f$). Similarly, if $V_{i,2} = (Y_{i,2}, Z_{i,2})$ is a vertex in S_f, then $V_{i,-2} = (-Y_{i,2}, Z_{i,2})$ is a vertex in S'_f. Using the symmetries of D_k, we can then generate the portion of $\mathcal{S}$ that forms the exterior of the balloon, i.e., that portion of the balloon that comes in contact with the atmosphere. In the following, we let $n_{i,1}$ be the vector normal to the curve $\mathcal{M}_1$ at vertex $v_{i,1}$, which is computed in the following way: If $e^{\perp}_{i,1}$ and $e^{\perp}_{i+1,1}$ are unit vectors in the xz plane perpendicular to $e_{i,1}$ and $e_{i+1,1}$, respectively, then

$$n_{i,1} = \frac{e^{\perp}_{i,1} + e^{\perp}_{i+1,1}}{\left|e^{\perp}_{i,1} + e^{\perp}_{i+1,1}\right|}, \qquad i = 2, \ldots, n_c + 1$$

By convention, $n_{i,1}$ is chosen to be the inward-pointing unit vector. Note that $n_{i,1} \cdot f_{i,12}$ is not necessarily zero.

Vertices $u_{i,0}$ form the crease of the internal fold in $\mathcal{S}_f$ and are computed as

$$u_{i,0} = v_{i,1} - \alpha_i n_{i,1}$$

By construction, $\alpha_i = |u_{i,0} - v_{i,1}| = |v_{i,0} - v_{i,1}|$. In previous work, e.g., Ref. 7, $v_{i,1}$ was determined by projecting $v_{i,2}$ onto the xz plane and α_i was a parameter to be determined. If the ith circumferential fiber is under sufficient tension, then $\alpha_i = 0$. Note that $f_{i,12}$ need not be parallel to $\boldsymbol{j} = (0, 1, 0)$. Unlike previous work where we required the length of each circumferential fiber to be fixed [see Eq. (2) of Ref. 10], a stretching or contraction of C_i is allowed in the present model.

In the flat reference configuration, we define

$$V_{i,1} = V_{i,0} + \frac{\alpha_i}{\alpha_i + |f_{i,12}|} C_i \tag{4}$$

where $i = 1, \ldots, n_c + 1$. Following our labeling convention, if $V_{i,1} = (Y_{i,1}, Z_{i,1})$, then $V_{i,-1} = (-Y_{i,1}, Z_{i,1})$. We define $F_{i,12} = V_{i,1} - V_{i,2}$, and so $F_{i,12}$ in the flat reference configuration is identified with $f_{i,12}$ in the deformed configuration. Note that both $V_{i,-1}$ and $V_{i,1}$ are identified with $v_{i,1}$, and the vertex $V_{i,0}$ is identified with $v_{i,0}$. When $\alpha_i = 0$, then $V_{i,-1} = V_{i,1} = V_{i,0}$ and $v_{i,1} = v_{i,0}$. By construction, $\alpha_1 = \alpha_{n_c+2} = 0$.

The design, i.e., float, shape is a surface of revolution generated by a curve,

$$\gamma_d(s) = (R_d(s), 0, Z_d(s)), \qquad 0 \le s \le \ell_d \tag{5}$$

that is found by solving the standard Σ-shape model equations. The design shape used here is based on a variation of the natural shape, where the cap weight is modeled as an added thickness. Before computing an EM shape, we define an unstrained curved configuration and its corresponding flat reference configuration for a half-gore. The unstrained curved shape of a half-gore is obtained by intersecting the parametrized ruled surface $X(s, v) = \gamma_d(s) + v\boldsymbol{j}$, where $\boldsymbol{j} = (0, 1, 0)$, $v \in R$, and the wedge-shaped region $\mathcal{W}_k$.

Partitioning the interval $[0, \ell_d]$, we have $0 = s_1 < s_2 < \cdots < s_{n_c+1} < s_{n_c+2} = \ell_d$. To be consistent with the way in which a real gore is constructed, we define

$$r_i = R_d(s_i)/\cos(\pi/k), \qquad z_i = Z_d(s_i) \tag{6}$$

$i = 1, \ldots, n_c + 2$, and the following:

$$\begin{gathered} \triangle r_i = r_{i+1} - r_i, \qquad \triangle z_i = z_{i+1} - z_i \\ \triangle s_i = \left[(\triangle r_i)^2 + (\triangle z_i)^2\right]^{\frac{1}{2}}, \qquad \triangle Y_i = |Y_{i+1,2} - Y_{i,2}| \end{gathered} \tag{7}$$

$$\triangle Z_i = \left[(\triangle s_i)^2 - (\triangle Y_i)^2\right]^{\frac{1}{2}} \tag{8}$$

for $i = 1, \ldots, n_c + 1$, where

$$Y_{i,2} = r_i \sin(\pi/k), \qquad i = 1, \ldots, n_c + 2 \tag{9}$$

Setting $Z_{1,2} = 0$ and using Eqs. (6–9), we obtain

$$Z_{i,2} = Z_{1,2} + \sum_{k=1}^{i} \triangle Z_k, \qquad i = 2, \ldots, n_c + 2 \tag{10}$$

Note that the total length of a gore's edge in the reference configuration is

$$L_d = \sum_{i=1}^{n_c+1} \triangle s_i$$

and, in general, is different from the arc length ℓ_d used to parameterize Eq. (5).

The initial configuration of the balloon shape is triangulated. A superscript 0 of a vertex label indicates that the vertex is in the (unstrained) initial configuration. In particular, vertices in the unstrained triangulation are given by

$$v^0_{i,2} = (r_i \cos(\pi/k), r_i \sin(\pi/k), z_i) \tag{11}$$

$$v^0_{i,1} = (r_i \cos(\pi/k), 0, z_i) \tag{12}$$

for $i = 1, \ldots, n_c + 2$. By construction, $\alpha_i^0 = 0$ and $v_{i,1}^0 = v_{i,0}^0 = v_{i,-1}^0$ for all i, and the $v_{i,1}^0$ lie on the generating curve given by Eq. (5). Vertices in the flat reference configuration are given by

$$V_{i,2} = (Y_{i,2}, Z_{i,2}) \tag{13}$$

$$V_{i,0} = (0, Z_{i,2}) \tag{14}$$

A typical fundamental section generated by the set $\{v_{i,j}\}$ will be denoted $\mathcal{S}_f = \mathcal{S}_f(v_{i,j})$. We can consider $\mathcal{S}_f$ and $\tilde{\mathcal{S}}_f$ as parameterized by the same set of vertices $\{v_{i,j}\}$ because the $u_{i,0}$ can be determined from the $v_{i,j}$. The initial unstrained configuration is denoted by $\mathcal{S}_f^0 = \mathcal{S}_f(v_{i,j}^0)$. As the balloon shape evolves to equilibrium, the vertices $v_{i,j}$ can move, subject to the degrees of freedom described earlier.

Each triangle in the deformed configuration $\mathcal{T}_l$ is identified with a triangle in the reference configuration T_l (see Figs. 2–4). If we let $N_\mathcal{T}$ denote the total number of facets in a triangulation of a fundamental section, we have

$$\mathcal{S}_f = \bigcup_{l=1}^{N_\mathcal{T}} \mathcal{T}_l \tag{15}$$

We can partition the set $\mathcal{T}_f = \{\mathcal{T}_l, l = 1, \ldots, N_\mathcal{T}\}$ into two disjoint subsets $\mathcal{T}_f^o$ and $\mathcal{T}_f^i$, where $\mathcal{T}_f^o$ denotes the set of triangles that form the exterior of the balloon and $\mathcal{T}_f^i$ denotes the set of triangles that form the internal folds. For the range of volumes considered here, the triangles $\mathcal{T}_f^o$ are those on which the atmospheric pressure acts. The triangles $\mathcal{T}_f^i$ correspond to regions of external contact (the outside of the balloon contacts itself). Note that triangles in $\mathcal{T}_f^o$ are constructed from the sets $\{v_{i,1}\}$ and $\{v_{i,2}\}$, whereas triangles in $\mathcal{T}_f^i$ are constructed from $\{u_{i,0}\}$ and $\{v_{i,1}\}$. We let $N_\mathcal{T}^o$ denote the number of triangles in $\mathcal{T}_f^o$ and $N_\mathcal{T}^i$ denote the number of triangles in $\mathcal{T}_f^i$. Without loss of generality, we can assume that the triangles $\mathcal{T}_l$ are numbered so that

$$\begin{aligned} \mathcal{T}_l &\in \mathcal{T}_f^o, \qquad \text{for } l = 1, \ldots, N_\mathcal{T}^o \\ \mathcal{T}_l &\in \mathcal{T}_f^i, \qquad \text{for } l = N_\mathcal{T}^o + 1, \ldots, N_\mathcal{T} \end{aligned} \tag{16}$$

where $N_\mathcal{T} = N_\mathcal{T}^i + N_\mathcal{T}^o$. The triangles are labeled from bottom to top. A similar convention will apply to triangles T_l and the reference configuration (see Fig. 2). In particular, we let

$$S_f = \bigcup_{l=1}^{N_\mathcal{T}} T_l$$

denote the preimage of $\mathcal{S}_f$. A similar decomposition could be carried out for $\tilde{\mathcal{S}}_f$. Following the same conventions, we could define $\tilde{\mathcal{T}}_f^o$ and $\tilde{\mathcal{T}}_f^i$, noting $\mathcal{T}_f^o = \tilde{\mathcal{T}}_f^o$, but $\mathcal{T}_f^i \neq \tilde{\mathcal{T}}_f^i$ because $\{v_{i,0}\}$ and $\{v_{i,1}\}$ are used to form the facets $\mathcal{T}_f^i$. By construction, $N_\mathcal{T}^o = N_\mathcal{T}^i = 2n_c$, and we say that T_{2q}, T_{2q+1} are adjacent in S_f.

A typical balloon system will include a number of external caps. For results presented here, the balloon contains two caps. These are modeled as an added thickness. To facilitate the mathematical description of caps, we partition the collection of facets S_f into three disjoint sets (see Fig. 2), $S_f = S_f^1 \cup S_f^2 \cup S_f^3$. If a facet $T_l \in S_f^\tau$, then T_l contains τ layers of film. For any $T_l \in S_f$, we define the integer valued function

$$\omega(T_l) = \tau, \qquad \text{for } T_l \in S_f^\tau, \qquad \tau \in \{1, 2, 3\} \tag{17}$$

It is possible to model caps with different film material properties by modifying our approach. However, in our applications, each layer of film is assumed to have identical physical properties.

III. Problem Formulation

The inclusion of strain energy in our analysis of balloon shapes is done through a variational principle, assuming a constant strain model for the balloon film and a linearly elastic string model for the load tapes. In the following section, we will outline our variational approach. Strain energy was included in Ref. 7, but only float shapes were considered and the geometry was restricted to maintain a ruled surface for the portion of the gore that contacts the atmosphere. Ascent shapes in the range $0.91 \leq \mathcal{V}/\mathcal{V}_d \leq 1$ were considered in Ref. 3 using a model with fewer degrees of freedom.

The total potential energy of a balloon configuration, E_{total}, is the sum of six terms,

$$E_{\text{total}} = E_{\text{gas}} + E_{\text{film}} + E_{\text{tape}} + E_{\text{top}} + S_{\text{tapes}} + S_{\text{film}} \tag{18}$$

where E_{gas} is the potential energy due to the lifting gas, i.e., the hydrostatic pressure potential; E_{film} is the gravitational potential energy of the film; E_{tape} is the gravitational potential energy of the load tapes; E_{top} is the gravitational potential energy of the top fitting; S_{tapes} is the strain energy of the load tapes; and S_{film} is the strain energy of the balloon film. In the following sections, we give a brief description of each of these quantities and indicate how they are computed numerically.

A. Hydrostatic Pressure Potential

For a balloon at a fixed altitude, it is reasonable to assume that the densities of the lifting gas and ambient air (ρ_{gas} and ρ_{air}, respectively) are constant over the height of the balloon. In this case, the pressure difference across the balloon film at level z is given by

$$P = -g(\rho_{\text{air}} - \rho_{\text{gas}})(z - z_0) \tag{19}$$

where g is acceleration due to gravity and z_0 indicates the location of the zero-pressure level, e.g., see Eq. (7), p. II.5, Ref. 12. The specific buoyancy at float will be denoted by $b_d = g(\rho_{\text{air}} - \rho_{\text{gas}})$. In this work, we assume that $z_0 = 0$ for our EM shapes. In this case, the potential energy of the lifting gas is given by

$$E_{\text{gas}} = -b_d \iiint_\mathcal{V} z \, \mathrm{d}V \tag{20}$$

where $\mathcal{V}$ is the region occupied by the gas bubble. Equation (20) is the potential for hydrostatic pressure.[13] Using the divergence theorem and the symmetries of $\mathcal{S}$, Eq. (20) can be replaced by a sum of surface integrals[11]

$$E_{\text{gas}} = -2kb_d \sum_{l=1}^{N_\mathcal{T}^o} \int_{\mathcal{T}_l} \frac{1}{2} z^2 \boldsymbol{k} \cdot \mathrm{d}\boldsymbol{A} \tag{21}$$

where $\mathrm{d}\boldsymbol{A} = \vec{n} \, \mathrm{d}A$, where $\vec{n}$ is normal to $\mathcal{S}$, $\mathrm{d}A$ is the surface area measure on $\mathcal{S}$, and ($\boldsymbol{k} = 0, 0, 1$). For triangular facets, terms in Eq. (21) can be computed exactly.

To reflect the denser atmosphere at a lower altitude corresponding to volume $\mathcal{V}$ when $\mathcal{V} < \mathcal{V}_d$, the coefficient b_d in Eq. (20) is replaced by

$$b = b_d \mathcal{V}_d / \mathcal{V} \tag{22}$$

For ascent shapes, we will assume that the zero pressure level remains at the base of the balloon.

B. Gravitational Potential Energy

The gravitational potential energy due to the weight of the balloon film is

$$E_{\text{film}} = \iint_\mathcal{S} w_{\text{film}} z \, \mathrm{d}S \tag{23}$$

where the film weight density is w_{film}. A cap is a subset of S that covers the top portion of the balloon. If the balloon system includes several caps, their contribution to the gravitational potential in Eq. (23) can be incorporated by appropriately modifying the film weight density. We will assume that one cap covers the top 29% of the balloon and a second covers the top 27%. Partitioning the collection of facets as described in Sec. II and using the function ω [see Eq. (17)], we obtain the following approximation for E_{film}:

$$E_{\text{film}} = 2kw_{\text{film}} \sum_{l=1}^{N_\mathcal{T}} \bar{z}_l \omega(T_l) \, \text{area}(T_l) \tag{24}$$

where $\bar{z}_l$ is the z component of the centroid of $\mathcal{T}_l$.

The gravitational potential energy due to the weight of the load tapes is

$$E_{\text{tape}} = k w_{\text{tape}} \int_0^{L_m} \alpha_2(s) \cdot \boldsymbol{k}\, \mathrm{d}s$$

where w_{tape} is the load tape weight density, $\alpha_2(s) \in R^3$ for $0 \le s \le L_d$ is a parameterization of the curve $\mathcal{M}_2$, s is the arc length in the flat reference configuration, and $\boldsymbol{k} = (0, 0, 1)$. The z component of the centroid corresponding to the edge $e_{i,2}$ is $\bar{z}_{i,2} = \frac{1}{2}(z_{i+1,2} + z_{i,2})$. The contribution to the gravitational potential of this segment is $w_{\text{tape}} \bar{z}_{i,2} |E_{i,2}|$, where $E_{i,2}$ is defined in Eq. (1). The energy of $\mathcal{M}_2$ is

$$w_{\text{tape}} \sum_{i=1}^{n_c+1} \bar{z}_{i,2} |E_{i,2}|$$

The gravitational potential energy of the load tapes in a complete shape is

$$E_{\text{tape}} = k w_{\text{tape}} \sum_{i=1}^{n_c+1} \bar{z}_{i,2} |E_{i,2}| \tag{25}$$

C. Load Tape Strain Energy

We assume that a fiber segment in a load tape behaves like a linearly elastic string with stiffness constant K_{tape}. If s^* denotes the arc length along a deformed meridional fiber and s the corresponding arc length in the undeformed state, the nonlinear strain is given by $\varepsilon = (\mathrm{d}s^{*2} - \mathrm{d}s^2)/(2\mathrm{d}s^2)$ (see p. 58, Ref. 14). In the case of a linearly elastic string, we can assume that $(\mathrm{d}s^* + \mathrm{d}s)/(2\mathrm{d}s) \approx 1$, in which case we have $\varepsilon \approx (\mathrm{d}s^* - \mathrm{d}s)/\mathrm{d}s$. In our applications, the fiber segments are straight lines, and so the linearized strain of the ith segment in $\mathcal{M}_2$ is

$$\varepsilon_i = (|e_{i,2}| - |E_{i,2}|)/|E_{i,2}|, \qquad i = 1, \ldots, n_c + 1 \tag{26}$$

where $E_{i,2}$ and $e_{i,2}$ are defined in Eqs. (1) and (2), respectively. The corresponding strain energy for the ith segment of the load tape running along $\mathcal{M}_2$ with stiffness constant K_{tape} is $\frac{1}{2} K_{\text{tape}} (\varepsilon_i)^2 |E_{i,2}|$. Normally, for a linearly elastic cable, the tension is given by $T = A E_{\text{cable}} (S - S_0)/S_0$ (p. 18, Ref. 14). A is the cross-sectional area of the cable, and E_{cable} is the modulus of elasticity of the cable. A load tape consists of several polyethylene fibers. The value for K_{tape} is determined experimentally and is equivalent to $A E_{\text{cable}}$, having the units of pound force (lbf). It follows that the strain energy of the load tapes in a complete shape is

$$S_{\text{tapes}} = \frac{1}{2} k K_{\text{tape}} \sum_{i=1}^{n_c+1} (\varepsilon_i)^2 |E_{i,2}| \tag{27}$$

D. Balloon Film Strain Energy

In what follows, we will assume that the balloon film is made up of a single layer. Using the function ω defined in the preceding section, we will add the contribution of the caps. In our work, we will use a standard measure of shell strain energy, e.g., Eq. (1.1.20) of Ref. 4. However, because the balloon film has negligible bending stiffness, we drop terms related to the bending energy. Retaining only the first integral in Eq. (1.1.20) of Ref. 4 and assuming a linearly elastic isotropic material, the film strain energy S_{film} can be written as

$$S_{\text{film}} = \frac{1}{2} \int\!\!\int_{\Omega} \boldsymbol{n}(\boldsymbol{u}) : \gamma(\boldsymbol{u})\, \mathrm{d}A^0 \tag{28}$$

where $\boldsymbol{n}$ is the tensor of tangential stress resultants, γ is the Cauchy–Green strain tensor, : is the tensor inner product, and Ω is the parameter space for the flat reference configuration.[7] The vector field $\boldsymbol{u}$ in Eq. (28) denotes the displacement field that maps a triangle in the reference configuration to one in the deformed configuration. We will not use $\boldsymbol{u}$ directly in our derivation of an expression for S_{film}, but we will compute the contribution to S_{film} for a typical facet and then sum the results to obtain an approximation of the total strain energy of $\mathcal{S}$. The contravariant components of $\boldsymbol{n}$ are denoted by $n^{\alpha\beta}$ and $\boldsymbol{n} : \gamma = n^{\alpha}_{\beta} \gamma^{\beta}_{\alpha}$, where

$$n^{\alpha\beta} = E^{\alpha\beta\lambda\mu} \gamma_{\lambda\mu} \tag{29}$$

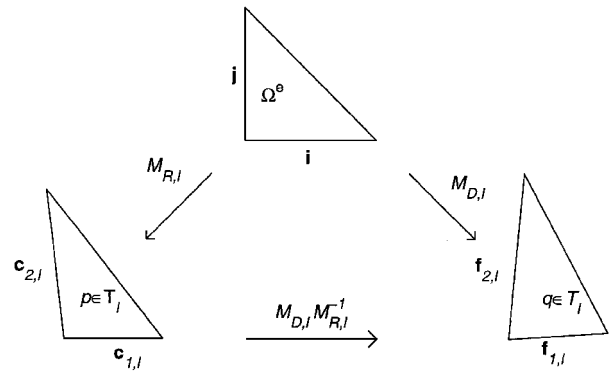

Fig. 5 Standard triangle Ω^e and the mapping, $q = M_{D,l} M_{R,l}^{-1} p$.

$E^{\alpha\beta\lambda\mu}$ is the tensor of elastic moduli, i.e.,

$$E^{\alpha\beta\lambda\mu} = \frac{eE}{2(1+\nu)} \left[a^{\alpha\lambda} a^{\beta\mu} + a^{\alpha\mu} a^{\beta\lambda} + \frac{2\nu}{1-\nu} a^{\alpha\beta} a^{\lambda\mu} \right] \tag{30}$$

where $a_{\alpha\beta} = \delta^{\beta}_{\alpha}$ is the first fundamental form of the reference configuration. Because we use flat facets, the second fundamental form $b_{\alpha\beta}$ is zero on each triangle.

To derive an expression for the strain energy, we define all of the geometric and physical quantities for a typical facet. Let $p \in T_l$ and $q \in \mathcal{T}_l$. Let $M_{R,l}$ be the linear map that takes a standard triangle Ω^e with sides $\boldsymbol{i} = (1, 0)$ and $\boldsymbol{j} = (0, 1)$ to $T_l \in S_f$, and let $M_{D,l}$ be the linear map that takes the Ω^e to a triangle in the deformed configuration $\mathcal{T}_l$. The mapping $p \to q$ is given by

$$q = M_{D,l} M_{R,l}^{-1} p$$

as shown in Fig. 5. The sides of T_l are $\boldsymbol{c}_{1,l}$ and $\boldsymbol{c}_{2,l}$, and these are identified with $\boldsymbol{f}_{1,l}$ and $\boldsymbol{f}_{2,l}$, the corresponding sides of $\mathcal{T}_l$. Because the mapping $p \to q$ is linear, the deformation gradient on the lth facet is

$$\boldsymbol{F}_l = \frac{\partial q}{\partial p} = M_{D,l} M_{R,l}^{-1}$$

In matrix form, the Cauchy strain is

$$\boldsymbol{C}_l = \boldsymbol{F}_l^T \boldsymbol{F}_l$$

the Cauchy–Green strain is

$$\mathbf{E}_l = \tfrac{1}{2}(\boldsymbol{C}_l - \boldsymbol{I})$$

and the tensor of tangential stress resultants is

$$\boldsymbol{N}_l = [eE/(1-\nu^2)][(1-\nu)\boldsymbol{E}_l + \nu\, \mathrm{tr}(\boldsymbol{E}_l)\boldsymbol{I}]$$

The matrices $\boldsymbol{N}_l$ and $\boldsymbol{E}_l$ are symmetric. By the spectral representation, we have

$$\boldsymbol{N}_l = \mu_{1,l} \boldsymbol{n}_{1,l} \boldsymbol{n}_{1,l}^T + \mu_{2,l} \boldsymbol{n}_{2,l} \boldsymbol{n}_{2,l}^T$$

where $\boldsymbol{n}_{1,l}$ and $\boldsymbol{n}_{2,l}$ are orthonormal vectors. The eigenvalues of $\boldsymbol{N}_l$ (denoted by $\mu_{1,l}$ and $\mu_{2,l}$) are the principal stress resultants.[15] See Appendix A of Ref. 7 for a further discussion. Because $\boldsymbol{n}(\boldsymbol{u})$ and $\gamma(\boldsymbol{u})$ are constant on each T_l in a constant strain model, we can approximate Eq. (28) by

$$2k \sum_{l=1}^{N_T} \frac{1}{2} \int_{T_l} \boldsymbol{n}(T_l) : \gamma(T_l)\, \mathrm{d}A^0$$

The contribution of external caps can be added by using the function ω. In this case, the total strain energy (based on configuration $\mathcal{S}_f$) is

$$2k \sum_{l=1}^{N_T} \frac{1}{2} \omega(T_l) (\boldsymbol{N}_l : \boldsymbol{E}_l)\, \mathrm{area}(T_l) \tag{31}$$

where $\boldsymbol{n}(T_l) : \gamma(T_l) = \boldsymbol{N}_l : \boldsymbol{E}_l$. In Ref. 7, the deformed gore was modeled as a ruled surface and the strain energy was based on

Eq. (31). In our present work, we base our strain energy approximation on the auxiliary configuration $\tilde{\mathcal{S}}_f$, and so if $\mathcal{T}_l \in \mathcal{T}_f^i$, we let $\tilde{\boldsymbol{E}}_l$ and $\tilde{\boldsymbol{N}}_i$ represent the corresponding Cauchy–Green strain and tangential stress resultants, respectively. The film strain energy approximation based on $\tilde{\mathcal{S}}_f$ is

$$S_{\text{film}} = 2k \sum_{l=1}^{N_{\mathcal{T}}^o} \frac{1}{2}\omega(T_l)(\boldsymbol{N}_l : \boldsymbol{E}_l)\,\text{area}(T_l) + 2k \sum_{l=N_{\mathcal{T}}^o+1}^{N_{\mathcal{T}}} \frac{1}{2}\omega(T_l)(\tilde{\boldsymbol{N}}_l : \tilde{\boldsymbol{E}}_l)\,\text{area}(T_l) \tag{32}$$

where we use $\tilde{\boldsymbol{N}}_l$ and $\tilde{\boldsymbol{E}}_l$ for $N_{\mathcal{T}}^o + 1 \le l \le \boldsymbol{N}_{\mathcal{T}}$. By construction, $\tilde{\boldsymbol{N}}_l = \boldsymbol{N}_l$ and $\tilde{\boldsymbol{E}}_l = \boldsymbol{E}_l$ for $1 \le l \le N_{\mathcal{T}}^o$. In Sec. IV, we discuss our reasons for basing the strain energy of ascent shapes on $\tilde{\mathcal{S}}_f$.

E. Variational Principle

The discrete form of the total energy of $\mathcal{S}$ is denoted by $E(v_{i,j})$ and is obtained by substituting Eqs. (21), (24), (25), (27), and (32) into Eq. (18). In particular, we have

$$E(v_{i,j}) = E_{\text{gas}} + E_{\text{film}} + E_{\text{tape}} + S_{\text{tapes}} + S_{\text{film}} + z_{\text{top}} w_{\text{top}} \tag{33}$$

The last term is the gravitational potential due to the top fitting of the balloon (w_{top} is the weight of the fitting, and $z_{\text{top}} = z_{2,n_c+2}$ is its height of above the base).

The gas bubble is partitioned into tetrahedra, all of which have a common vertex located on the z axis inside the gas bubble. The lth tetrahedron has facet $\mathcal{T}_l$ as base, and its volume is $\mathcal{V}_l$. The total volume of the gas bubble $\mathcal{V}$ is constrained so that

$$\mathcal{V} - 2k \sum_{l=1}^{N_{\mathcal{T}}^o} \mathcal{V}_l = 0 \tag{34}$$

Upper and lower bounds in the form

$$\begin{aligned} v_{i,0}^{\text{lb}} \le v_{i,0} \le v_{i,0}^{\text{ub}}, \qquad & i = 2, \ldots, 2n_c + 1 \\ v_{i,2}^{\text{lb}} \le v_{i,2} \le v_{i,2}^{\text{ub}}, \qquad & i = 2, \ldots, 2n_c + 1 \end{aligned} \tag{35}$$

are imposed. Vector inequalities are interpreted componentwise, and bounds in Eq. (35) are applied only to free parameters. The upper and lower bounds are chosen sufficiently large so they do not affect the solution. The variational principle that is used to compute the numerical EM shapes presented in Sec. IV is given by the following. Problem ($\star$): For $\mathcal{S}(v_{i,j}) \in \mathcal{C}_k$, minimize: $E(v_{i,j})$, subject to $G(v_{i,j}) = 0$, satisfying Eq. (35), where G is defined by the left-hand side of Eq. (34). MATLAB software (constr) is used to solve Problem ($\star$). Strictly speaking, the bounds in Eq. (35) are not required by constr. However, from a practical standpoint, specifying Eq. (35) accelerates the solution process by reducing the size of the set of feasible solutions.

IV. Numerical Solutions

For our calculations, we will consider a 29.5×10^6 ft^3, two-cap balloon based on a standard large scientific balloon design. The particular design is based on a variation of the natural shape, where the caps are modeled as added thickness and the tail of the gore is tapered. The balloon film is 0.8-mil polyethylene. We use a specific buoyancy that corresponds to a float altitude of 129,362 ft (see p. 73 of Ref. 5). Material constants such as Poisson's ratio ν, Young's modulus E, and load tape stiffness K_{tape} are highly temperature dependent, and we use values appropriate for the float condition, i.e., $E = 35{,}969$ psi, $\nu = 0.82$, and $K_{\text{tape}} = 5900$ lbf. The payload is adjusted appropriately so that the balloon is in equilibrium at float. Here, the payload includes the weight of the venting ducts, fins, inflation tubes, backup tapes, etc. For our design shape, the payload is 3559 lbf, the total film weight is 2509 lbf, the total tape weight is 520 lbf, and the weight of the top fitting is 30 lbf; see Table 1 for additional parameter values.

For our computations, we assume 38 circumferential fibers ($n_c = 38$) uniformly distributed along a meridian at intervals of roughly 15.3 ft. The results of our computations are summarized in Table 2, where we present data on a strained float shape ($\mathcal{V}/\mathcal{V}_d = 1.0$) and strained ascent shapes ($0.22 \le \mathcal{V}/\mathcal{V}_d < 1.00$). To compute the strained float shape, we use the unstrained curved reference configuration as an initial guess and solve Problem ($\star$). We then decrement the volume in steps of size (at most) $\triangle\mathcal{V} = -0.015\mathcal{V}_d$ and compute an energy-minimizing shape at each stage, using the EM shape from the previous step as the starting shape for the current target volume. We find that, if we try to change the volume by too large an amount, the solution process would diverge.

Table 1 Parameter values

Description	Variable	Value
Young's modulus, psi	E	35,969
Poisson's ratio	ν	0.82
Film weight density, lbf/ft^2	w_{film}	0.0038400
Load tape weight density, lbf/ft	w_{tape}	0.0054835
Load tape stiffness parameter, lbf	K_{tape}	5,900
Film thickness, in.	e	0.0008
Specific buoyancy at float, lbf/ft^3	b_d	2.2539e-4
Volume at float, 10^6 ft^3	$\mathcal{V}_{\text{float}}$	29.5
Number of gores	n_g	159
Design gore length, ft	ℓ_d	596.859

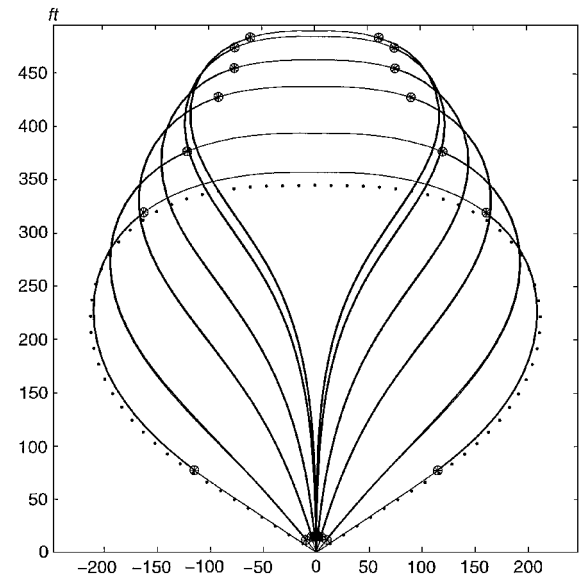

Fig. 6 Unstrained design shape (. . . .), strained shapes (——); $0.22 \le \mathcal{V}/\mathcal{V}_d \le 1.00$; ⊗ marks the range of the fold.

In Fig. 6, we present profiles of the design shape and the strained EM shape corresponding to $0.22 \le \mathcal{V}/\mathcal{V}_d \le 1.00$. The principal stress resultants of the two exterior triangles located at the same station are averaged, and it is this average value that is plotted in Figs 7. We denote the averaged principal stress resultants by $\hat{\mu}_{r,q}$, where $\hat{\mu}_{r,1} = \mu_{r,1}$, $\hat{\mu}_{r,n_c} = \mu_{r,2n_c}$:

$$\hat{\mu}_{r,q} = \tfrac{1}{2}(\mu_{r,2q} + \mu_{r,2q+1}), \qquad r = 1, 2$$

for $q = 2, \ldots, n_c - 1$. In S_f, the triangles T_{2q} and T_{2q+1} form a quadrilateral, and we can interpret $\hat{\mu}_{r,q}$ as measured at the centroid of the qth quadrilateral. (Note that $\mathcal{T}_{2q}$, $\mathcal{T}_{2q+1}$ need not lie in the same plane.) Following the numbering scheme already introduced, averaged principal stress resultants can be computed for interior quadrilaterals of excess material. We observe by examining the eigenvectors corresponding to $\mu_{1,l}$ and $\mu_{2,l}$ that $\mu_{1,l}$ corresponds to the circumferential direction and $\mu_{2,l}$ corresponds to the meridional direction for the float configuration. However, for ascent shapes, the direction of the principal stress resultants need not coincide with the meridional and circumferential directions. The corners in the graphs of the averaged principal stress resultants near $s = 400$ ft in Figs. 7 correspond to the edge of the caps. The corners are not present when the balloon is without caps.

Table 2 Strained EM shapes; units of energy are foot-lbf

Quantity	Design	$\mathcal{V}=\mathcal{V}_d$	$0.85\mathcal{V}_d$	$0.58\mathcal{V}_d$	$0.40\mathcal{V}_d$	$0.25\mathcal{V}_d$	$0.22\mathcal{V}_d$
S_{film}	0	3,310	2,673	1,814	1,677	1,627	1,617
S_{tapes}	0	7,575	3,754	2,850	2,898	3,075	3,098
E_{gas}	−1,356,014	−1,400,190	−1,655,352	−2,013,271	−2,259,769	−2,514,006	−2,575,507
E_{film}	599,929	632,681	710,374	790,186	826,349	852,913	858,160
E_{tape}	101,657	104,673	118,836	133,370	139,900	144,693	145,648
E_{top}	10,350	10,707	11,567.74	13,119	13,870	14,548	14,698
E_{total}	−654,426	−641,242	−807,904	−1,071,932	−1,275,073	−1,497,150	−1,552,285
$\max_i y_{i,1}$	0	0.0317	0.5110	1.4744	2.2249	2.9743	3.1153
δ_c^-	0	−0.0197	−0.0166	−0.0138	−0.0132	−0.01337	−0.013340
δ_c^+	0	0.00208	0.00178	0.00184	0.00217	0.002418	0.002685
δ_m^+	0	0.00500	0.00357	0.00314	0.003187	0.003289	0.003304
δ_d^-	0	0.00192	0.00166	0.00172	0.001959	0.00221	0.002403
δ_d^+	0	0.00665	0.00483	0.00397	0.003925	0.00434	0.004393
δ_d	0	0.00470	0.00378	0.00324	0.003238	0.00331	0.003328
θ_0, deg	57.460	56.431	39.994	17.421	6.6025	1.357	0.8300
z_{top}	345.00	356.902	393.632	437.290	462.343	484.939	489.935
$r_{1,\max}$	211.88	209.667	193.930	166.548	145.676	123.464	117.831
$r_{2,\max}$	211.93	209.708	193.716	166.406	145.549	123.431	117.802

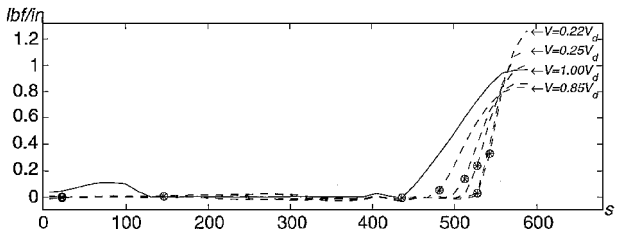

a) $\hat{\mu}_{1,q}$ circumferential

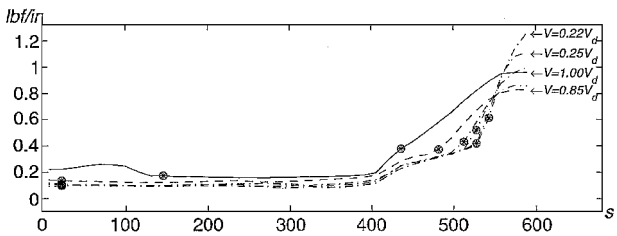

b) $\hat{\mu}_{2,q}$ meridional

Fig. 7 Averaged principal stress resultants, where s is arclength measured in reference configuration; $0.22 \le \mathcal{V}/\mathcal{V}_d \le 1.00$; ⊗ marks the range of the fold.

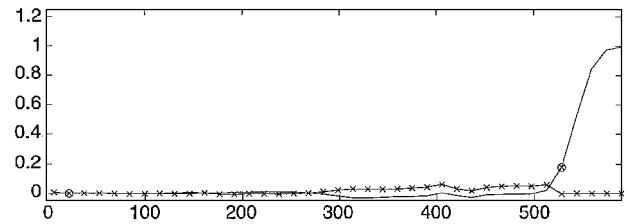

a) $\hat{\mu}_{1,q}$ circumferential

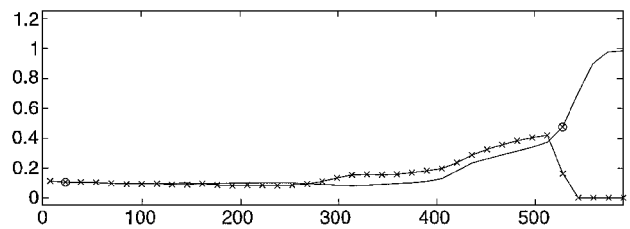

b) $\hat{\mu}_{2,q}$ meridional

Fig. 8 Averaged principal stress resultants, where s is arclength measured in reference configuration; outside facets (——), fold facets (–×–×–); $\mathcal{V}/\mathcal{V}_d = 0.36$; ⊗ marks the range of the fold.

Before discussing our numerical results, we first comment on the differences between solutions of Problem (⋆) when Eq. (31) (S_{film} based on $\mathcal{S}_f$ as in Ref. 7) and Eq. (32) (S_{film} based on $\tilde{\mathcal{S}}_f$) are used to evolve a strained float shape. If Eq. (32) is used, the corresponding energy minimizing shape is 0.1 ft taller and 0.4 ft smaller in diameter, the fold is about 45 ft longer, and the maximum fold depth is about the same (0.03 ft). Geometrically, the shapes $\mathcal{S}_f$ and $\tilde{\mathcal{S}}_f$ are the same. The total strain energy and the the maximum averaged meridional stress resultants are the same (0.95 lbf/in.) for both shapes. However, for triangles that bound the gas bubble, the circumferential stresses are higher in magnitude when Eq. (31) is used. The size of the fold is so small that corresponding stress resultants are unreliable. Whereas for strained float shapes we conclude that results based on $\tilde{\mathcal{S}}_f$ and on $\mathcal{S}_f$ are essentially the same, this is not the case as the volume decreases. If Eq. (31) is used for modeling ascent shapes, the circumferential stress resultants for solutions are greater in magnitude than the corresponding results for a solution based on Eq. (32). Whereas $\mathcal{S}_{\text{film}}$ decreases with decreasing volume using $\tilde{\mathcal{S}}_f$, when $\mathcal{S}_f$ is used, $\mathcal{S}_{\text{film}}$ increases with decreasing volume. Higher compressive stresses are observed in shapes based on Eq. (31). In addition, spikes in the principal stress resultants occur near the points where the internal fold initiates and terminates when the strain energy is based on $\mathcal{S}_f$. We believe this is due to the inability of the geometric model to adapt adequately to the equilibrium position. In observations of a demonstrator balloon, we noted transition areas that bridge subregions of external contact, i.e., folds, and regions of biaxial tension. Our model would not be able to handle such features. For the class of ascent shapes considered, we find that results based on $\tilde{\mathcal{S}}_f$ are more representative of how the real balloon behaves, and so Eq. (32) will be used to approximate the strain energy in the film for ascent shapes.

Figure 8 shows the averaged principal stresses for both the folded (interior) facets and exterior facets for the case $\mathcal{V}=0.36\mathcal{V}_d$. From Fig. 8, we see that, when an internal fold is present, the principal stress resultants of a fold are comparable to those of the adjacent exterior triangles (other cases in Table 2 are very similar). Figure 9 shows one-half of the load tape tension for each of our computed EM shapes. In Figs. 6–9, the points where the internal fold initiates and terminates are indicated with the symbol ⊗. On examining the strained float shape in Fig. 6, we find the balloon is slightly concave below the station where the internal fold initiates. This explains why both principal stress resultants are positive near the tail of the balloon. This is due to a tapering in the design shape. For the design that we used, the tail of the balloon is nearly that of a cone, and so there is very little excess material in this region at float. When the gores are not tapered [see, e.g., case I(b) of Ref. 7], we find that this behavior does not occur. In any case, this effect near the tail of the balloon at float is due to the design shape, not the solution process.

V. Discussion

At float conditions, we compute maximum principal stress resultants of approximately 1 lbf/in. Initially, as the volume decreases,

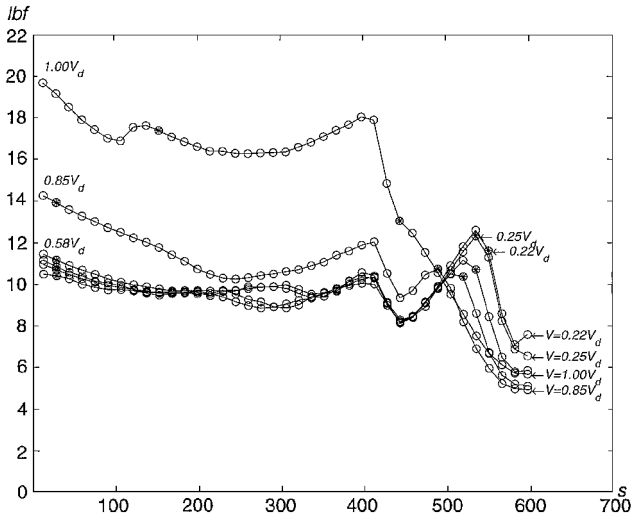

Fig. 9 One-half load tape tension for $0.22 \leq \mathcal{V}/\mathcal{V}_d \leq 1.00$; ⊗ marks the range of the fold.

we observe a drop in the maximum principal stress resultants for the corresponding ascent shapes (for $0.85 \leq \mathcal{V}/\mathcal{V}_d \leq 1.0$). This was also observed in Ref. 3, where a slightly different model was used. However, when the volume goes below a certain critical level, we see that the maximum principal stress resultants begin to rise in the region near the top of the gas bubble (see Fig. 7). This is not totally unexpected because the radius of curvature of a circumferential fiber decreases as the gas bubble is reduced. We find that the maximum principal stress resultants of shapes in the range $0.22 \leq \mathcal{V}/\mathcal{V}_d \leq 1.00$ occur when $\mathcal{V} = 0.22\mathcal{V}_d$. We find that, around $\mathcal{V} = 0.22\mathcal{V}_d$, the angle at the base of the balloon is approximately 0.83 deg, the internal fold penetrates the z axis, and the inside of the balloon comes into contact with itself. It is unlikely that one would see an ascent shape with $\mathcal{V} = 0.22\mathcal{V}_d$ as in Fig. 6. Internal contact probably occurs much earlier than $\mathcal{V} = 0.22\mathcal{V}_d$ due to other factors, such as imperfections introduced during the balloon's construction or the stretching of certain areas of the balloon while in the launch spool. In an actual flight, the balloon will assume an asymmetric shape, and so it is unlikely that one would see ascent shapes of the kind described here for low volumes. In fact, if the zero-pressure level lies above the base of the balloon, the differential pressure will act to push the film inward near the base of the balloon. Once internal contact takes place, most likely the balloon will assume a configuration with flat wing-like structures near its base, e.g., see Ref. 10. It might be interesting to compare the energy of strained ascent shapes (including those with wing sections) to determine whether there is a minimum energy principle that could help explain why configurations with a certain number of wing sections are observed more frequently than others.

In Fig. 6, we see that the strained balloon shape at float is about 12 taller than its design and about 4 ft smaller in diameter. In Fig. 7, we present plots of the averaged principal stress resultants of exterior facets for the strained float and ascent configurations. In Ref. 7, we found good qualitative and quantitative agreement when our results on the float configuration were compared to similar results using a more sophisticated finite element method code. This gives us a certain level of confidence for our results on partially inflated configurations.

As the volume decreases, the base angle of the balloon decreases. Consequently, the magnitude of the reaction force due to the payload decreases. This can be seen in Fig. 9, where one-half the load tape tension is presented. Initially, there is a corresponding overall reduction in the principal stress resultants in the balloon film ($0.85 \leq \mathcal{V}/\mathcal{V}_d \leq 1.0$). However, for $\mathcal{V}/\mathcal{V}_d < 0.58$, we find that the maximum principal stress resultants begin to rise in the region near the top of the balloon. The same effect is observed in Fig. 9 near $s = 500$ ft, where the maximum load tape tension increases with decreasing volume.

VI. Concluding Remarks

Because of the presence of internal folds of excess material, standard membrane theory cannot be directly applied to partially inflated balloon shapes. However, our energy minimizing approach is tailor-made to handle partially inflated configurations. Using our model, we can compute strained balloon shapes in the range $0.22 \leq \mathcal{V}/\mathcal{V}_d \leq 1.0$. We find that the maximum principal stresses in the film are experienced at $\mathcal{V}/\mathcal{V}_d = 0.22$. Even though the total strain energy of the balloon is lower at the lower volume, the maximum stresses are higher.

Although our work on modeling balloon shapes is motivated by zero-pressure designs, our results can be applied to superpressure designs or any other designs, fully or partially inflated.

Acknowledgment

The research presented in this paper was supported by NASA Grant NAG5-697.

References

[1]"Research and Development in the Field of High Altitude Plastic Balloons," Dept. of Physics, NONR-710(01) Repts., Univ. of Minnesota, Minneapolis, MN, 1951–1956.

[2]Baginski, F., Collier, W., and Williams, T., "A Parallel Shooting Method for Determining the Natural-Shape of a Large Scientific Balloon," *SIAM Journal on Applied Mathematics*, Vol. 58, No. 3, 1998, pp. 961–974.

[3]Baginski, F., and Collier, W., "Energy Minimizing Shapes of Partially Inflated Large Scientific Balloons," *Advances in Space Research*, Vol. 21, No. 7, 1988, pp. 975–978.

[4]Oden, J. T., and Carey, G. F., *Finite Elements. Special Problems in Solid Mechanics*, Vol. 5, Prentice–Hall, Englewood Cliffs, NJ, 1984, pp. 1–20.

[5]Warren, J. C., Smalley, J. H., and Morris, A. L., "Aerostatic Lift of Helium and Hydrogen in the Atmosphere," National Center for Atmospheric Research, NCAR-TN/IA-69, Boulder, CO, Dec. 1971.

[6]Oden, J. T., *Finite Elements of Nonlinear Continua*, McGraw–Hill, New York, 1972, Chap. 18.

[7]Baginski, F., and Collier, W., "A Mathematical Model for the Strained Shape of a Large Scientific Balloon at Float Altitude" (submitted for publication).

[8]Schur, W., "Recent Advances in the Structural Analysis of Scientific Balloons," Compendium of NASA Balloon Research and Development Activities for Fiscal Year 1992, NASA Balloon Projects, Wallops Flight Facility, Wallops Island, VA, 1992.

[9]Steigmann, D. J., "Tension-Field Theories of Elastic Membranes and Networks," *Recent Developments in Elasticity*, Applied Mechanical Div., Vol. 124, American Society of Mechanical Engineers, New York, 1991, pp. 41–49.

[10]Baginski, F., "Modeling Nonaxisymmetric Off-Design Shapes of Large Scientific Balloons," *AIAA Journal*, Vol. 34, No. 2, 1996, pp. 400–407.

[11]Baginski, F., and Ramamurti, S., "Variational Principles for Ascent Shapes of Large Scientific Balloons," *AIAA Journal*, Vol. 33, No. 4, 1995, pp. 764–768.

[12]Morris, A. L. (ed.), *Scientific Ballooning Handbook*, National Center for Atmospheric Research, NCAR-TN-99, Boulder, CO, 1975, Sec. V, pp. 1–45.

[13]Fisher, D., "Configuration Dependent Pressure Potentials," *Journal of Elasticity*, Vol. 19, 1988, pp. 77–84.

[14]Leonard, J. W., *Tension Structures*, McGraw–Hill, New York, 1988, pp. 18, 58.

[15]Antman, S. S., *Nonlinear Problems of Elasticity*, Springer–Verlag, New York, 1995.

R. K. Kapania
Associate Editor